Journal of Engineering and Technology for Industrial Applications

ITEGAM-JETIA

Manaus, v.12 n.58, p. 160-172. March/April, 2026.
DOI: https://doi.org/10.5935/jetia. v12i58.2934

ISSN ONLINE: 2447-0228

RESEARCH ARTICLE OPEN ACCESS

PERFORMANCE EVALUATION OF SOLAR PV-BATTERY HYBRID SYSTEM POWERED BLDC MOTOR SPEED CONTROL USING ULTRA-LIFT LUO-CONVERTER

G. Dilli Harsha[1], Dr. Vyza Usha Reddy[2]

[1, 2]Department of Electrical and Electronics Engineering, Sri Venkateswara University College of Engineering, Tirupati

[1]https://orcid.org/0009-0000-1786-9587, [2]http://orcid.org/0009-0004-7070-8925

Email: dilliharsha6@gmail.com, vyza_ushareddy@yahoo.co.in

ARTICLE INFO

Article History
Received: November 13, 2025
Reviewed: January 14, 2026
Accepted: January 22, 2026
Published: March 31, 2026

Keywords:
Ultra-lift Luo-converter,
Brush Less DC(BLDC) motor,
Bidirectional buck-boost converter,
Voltage Source Inverter (VSI),
Proportional–Integral Derivative (PID) controller

ABSTRACT

The increasing use of solar energy poses challenges in meeting energy demands due to its unpredictable weather conditions. With the growing need for electric drives, integrating solar energy with battery storage through advanced power electronic converters is essential to ensure system stability and energy sufficiency. This design proposes a solar photovoltaic (PV) array and battery-supported brushless DC (BLDC) motor drive capable of operating efficiently and reliably under varying solar irradiance and temperature conditions. The solar PV array output voltage is boosted to the level required by the motor using an ultra-lift Luo-converter, while a bidirectional buck–boost converter manages the power flow between the battery and the DC bus. The BLDC motor is driven by a three-phase voltage source inverter (VSI), whose electronic commutation is controlled using Hall sensor feedback. Motor speed control is achieved through a Proportional–Integral–Derivative (PID) controller designed for the ultra-lift Luo-converter. By addressing the effects of varying irradiance and temperature, the proposed system ensures stable operation. Due to its modular architecture and hybrid energy management capability, the system shows strong potential for applications in solar–battery-powered Computer Numerical Control (CNC) machines and standalone renewable energy systems. The performance evaluation of the proposed BLDC motor speed control system is carried out in MATLAB/Simulink.

I. INTRODUCTION

Solar photovoltaic (PV) technology has emerged as one of the most viable solutions to meet the increasing global demand for clean and sustainable energy [1]. Unlike conventional fossil fuels, solar PV systems do not emit harmful greenhouse gases. Therefore, solar PV can be considered an environmentally friendly option for mitigating climate change and enhancing energy security [2]. However, the primary limitation of solar energy is its unavailability during nighttime. This limitation can be overcome by integrating Energy Storage Systems (ESS) such as batteries.

BLDC motors have gained significant importance in modern electric drive systems due to their superior efficiency, performance, and reliability compared to conventional brushed motors. BLDC motors with trapezoidal back electromotive force (back-EMF) characteristics are particularly well-suited for applications requiring durability and long-term operational stability. By utilizing electronic commutation through power semiconductor switches, these motors ensure smooth torque delivery [3–5].

In recent years, DC–DC voltage-lift (VL) converters, such as the ultra-lift Luo-converter, have become highly significant in high-voltage DC applications like solar power generation and electric vehicles. The ultra-lift Luo-converter, proposed by F. L. Luo and H. Ye in 2004, is named after its inventor [6], [7]. This converter employs advanced voltage-lift technology to efficiently step up low input voltages to considerably higher output levels. Its compact and robust design makes it suitable for demanding consumer and industrial applications.

The bidirectional buck–boost converter is another DC–DC converter topology that allows power flow between two DC voltage sources. It can either step up (boost) or step down (buck) the voltage, depending on the operating mode, and is commonly employed in battery energy storage systems. To achieve the desired high-voltage output and stable performance, it is essential to incorporate a feedback controller. A properly designed feedback controller can enhance the dynamic response of the converter under varying load and irradiance conditions. This work focuses on the speed control of a BLDC motor using an ultra-lift Luo-converter fed by a solar PV–battery hybrid system operating under dynamic solar irradiance and temperature variations [8-10].

II. PROPOSED SYSTEM CONFIGURATION

The proposed system comprises a solar PV array, an ultra-lift Luo-converter, a bidirectional converter with battery storage, and a three-phase inverter that drives the BLDC motor (Figure 1). The solar PV array serves as the primary energy source, while the ultra-lift Luo-converter boosts the voltage to meet the motor's operational requirements. The bidirectional converter facilitates power exchange between the battery and the DC bus—charging the battery when excess solar power is available and discharging it during periods of low irradiance. The system can operate in three distinct modes:

(i) Solar PV-dominant mode: where the motor is powered directly by solar energy.
(ii) Standalone battery mode: where the battery alone supplies power to the motor.
(iii) Hybrid mode: where both solar PV and battery jointly supply power under transient solar conditions.

The working principle is governed by energy management system between the solar PV array and the battery. Under high solar irradiance, the generated energy is primarily used to drive the motor, and any excess power is stored in the battery. During low irradiance conditions, the battery supports the solar PV through the bidirectional converter to maintain stable operation. At night or under poor solar conditions, the battery alone supplies the required energy, ensuring continuous operation of the system.

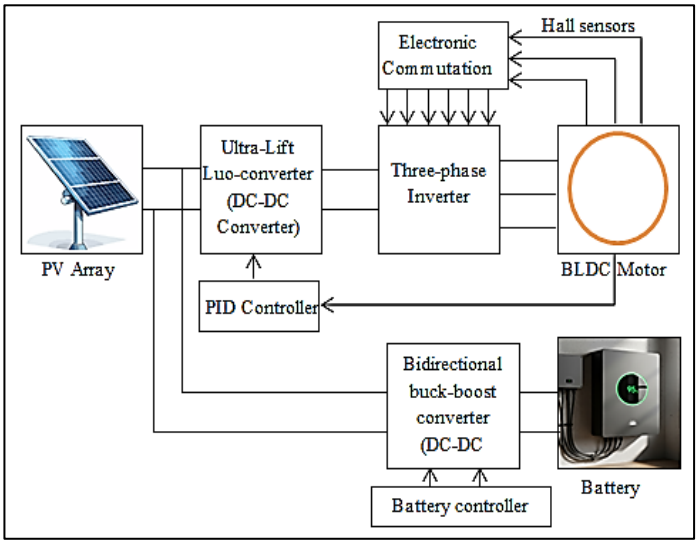

Figure 1: Proposed conFigureuration of Solar PV-Battery Hybrid Fed BLDC Motor Speed Control Using Ultra-Lift Luo-Converter.
Source: Authors, (2026).

III. DESIGN AND SPECIFICATIONS OF THE PROPOSED SYSTEM

III.1 PARAMETERS OF SOLAR PV ARRAY

The Tata Power Solar Systems TP300LBZ module is a well-established and widely utilized solar panel in distributed solar energy applications. It is a polycrystalline-type photovoltaic module designed to deliver a rated output power of 300 W under standard test conditions. This module contains 72 solar cells interconnected in series. The TP300LBZ module suits medium-voltage DC bus applications when several modules are connected together since it has an open-circuit voltage of 44.4 V and a short-circuit current of about 8.7 A. In order to achieve 1.2 kW, four modules are connected parallel.

Table 1: Ratings and specifications of PV System.

Array Configureuration	4 modules in parallel; 1 in series per string		
Nominal Power Output	300.12 W	**Temperature Coefficient of Voltage**	−0.33 %/°C
Open-Circuit Voltage	44.4 V	**Temperature Coefficient of Current**	0.063797 %/°C
Voltage at Peak Power	36.6 V	**Photogenerated Current**	8.7148 A
Total Cells per Module	72	**Reverse Saturation Current**	9.9881×10^{-11} A
Short-Circuit Current	8.69 A	**Diode Quality Factor**	0.9533
Current at Rated Power	8.20 A	**Series Path Resistance**	0.30152 Ω
Shunt Path Resistance	360.7804 Ω		

Source: Authors, (2026).

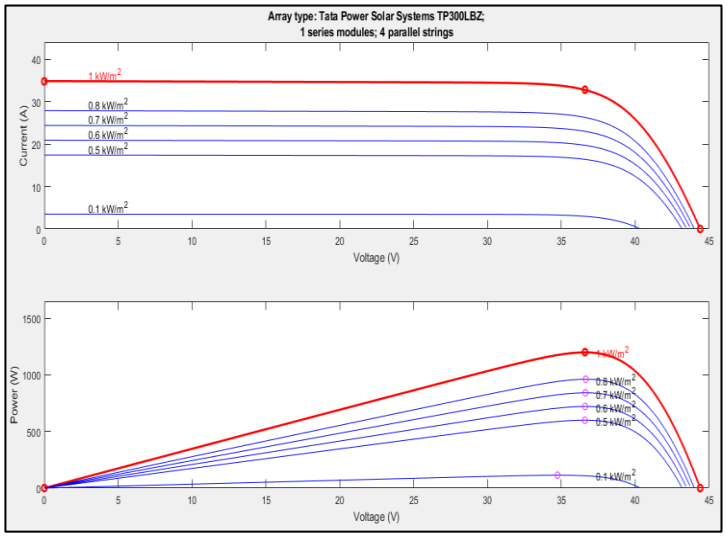

Figure 2: I-V & P-V characteristics of Tata Power Solar Systems TP300LBZ.
Source: Authors, (2026).

Irradiance and temperature at latitude 13.6281^{0}N longitude 79.3953^{0}E (SVUCE EEE block, Tirupati) on 21st June 2024(longest day in the year) provided to the PV array as inputs. Irradiance and temperature data is represented in following Figure 3.

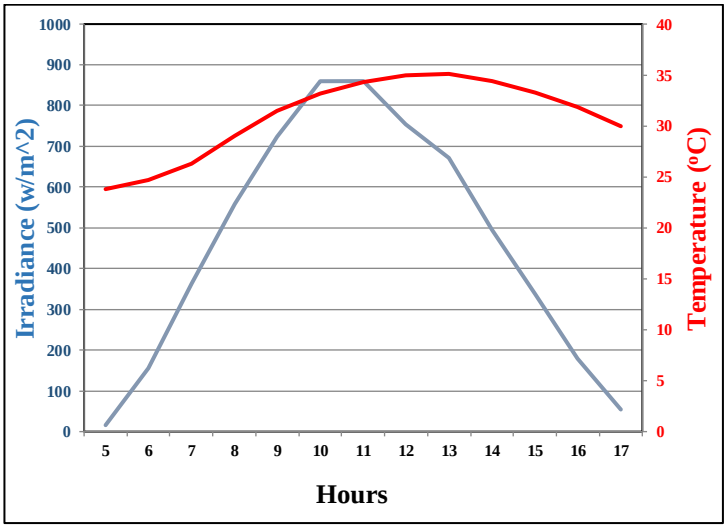

Figure 3: Hourly based irradiance and temperature data on 21st June 2024 at 13.6281^{0}N, 79.3953^{0}E.
Source: Authors, (2026).

III.2. ULTRA-LIFT LUO-CONVERTER

The ultra-lift Luo-converter (Figure 4), which comprises a MOSFET switch (S), two inductors (L_1 and L_2), two capacitors (C_1 and C_2), three diodes (D_1, D_2, D_3), and a resistive load denoted as R. To elucidate the operation of the ultra-lift Luo-converter, it is assumed that all diodes and the switch S are ideal components.

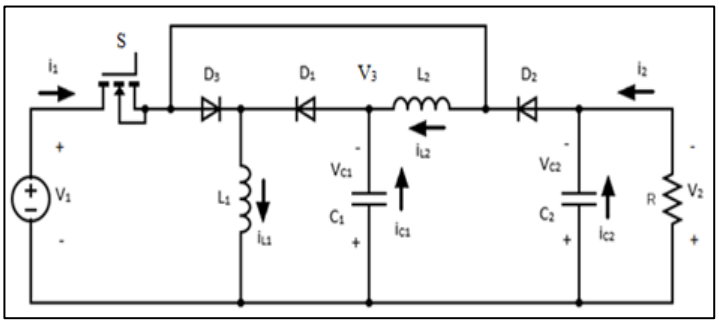

Figure 4: Ultra-lift Luo-converter.
Source: Authors, (2026).

Operation modes of ultra-lift Luo-converter are:

1. Continuous-Conduction-Mode (CCM)
2. Discontinuous-Conduction-Mode (DCM)

1. Continuous-Conduction-Mode (CCM)

When the control switch is activated, diode D_3 becomes forward-biased, while diodes D_1 and D_2 are reverse-biased, causing inductors L_1 and L_2 to charge and capacitors C_1 and C_2 to discharge as illustrated in Figure 5**.**

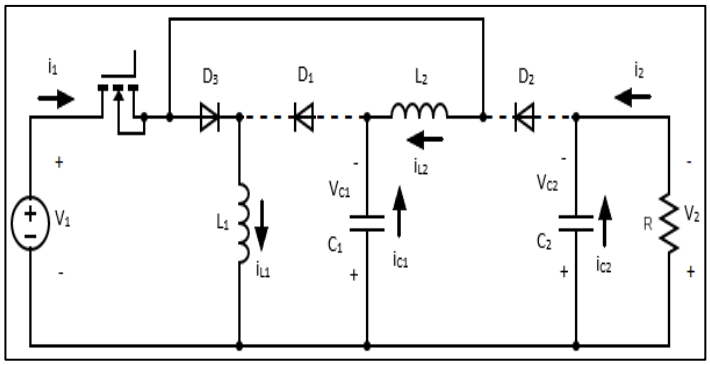

Figure 5: Ultra-lift Luo-converter equivalent circuit during switch- ON period.
Source: Authors, (2026).

When the control switch is deactivated, diode D_3 becomes reverse-biased, whereas diodes D_1 and D_2 become forward-biased, causing inductors L_1 and L_2 to discharge and capacitors C_1 and C_2 to charge, as shown in Figure 6**.**

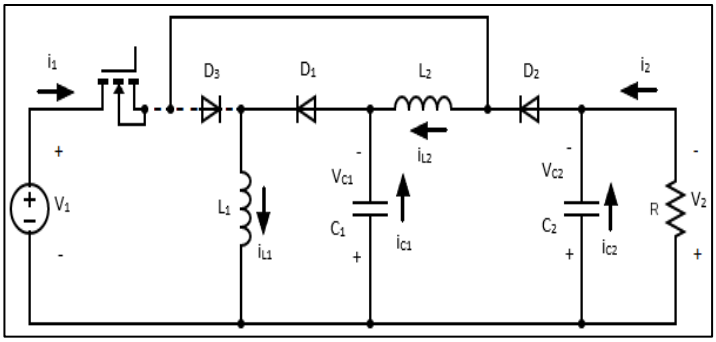

Figure 6: Ultra-lift Luo-converter equivalent circuit during switch- OFF period.
Source: Authors, (2026).

2. Discontinuous-Conduction-Mode (DCM)

The operation in discontinuous is same as the operation during switch-OFF condition (Figure 8) except inductor current i_{L1} falls to zero for short period of time as shown in Figure 7.

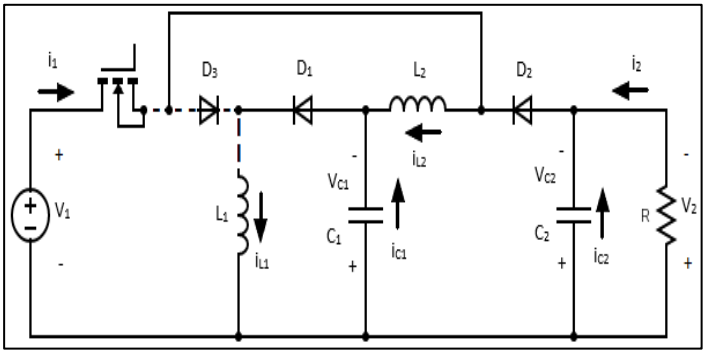

Figure 7: Ultra-lift Luo-converter equivalent circuit during discontinuous conduction mode.
Source: Authors, (2026).

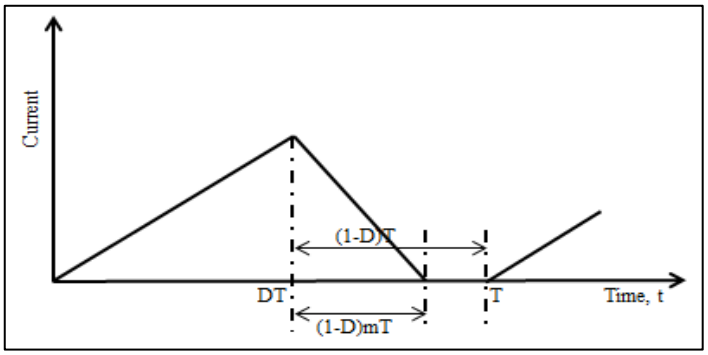

Figure 8: Discontinuous inductor current i_{L1}.
Source: Authors, (2026).

III.2.1 Analysis of Ultra-Lift Luo-Converter

Voltage gain, $G=\frac{V_2}{V_1}=\frac{D*(2-D)}{(1-D)^2}$

Ripple current through L_1, $\Delta i_{L1} = \frac{DT*V_1}{L_2}$

Ripple current through L_2, $\Delta i_{L2} = \frac{DT*V_1}{(1-D)*L_2}$

Ripple voltage across C_1, $\Delta v_{C1} = \frac{DT*I_2}{(1-D)*C_1}$

Ripple voltage across C_2, $\Delta v_{C2} = \frac{DT*I_2}{C_2}$

For discontinuous conduction mode (DCM),

Inductor L_1 current variation ratio, $\varepsilon_1 = \frac{\Delta i_{L1}/2}{I_{L1}} > 1$

Inductor L_2 current variation ratio, $\varepsilon_2 = \frac{\Delta i_{L2}/2}{I_{L2}} > 1$

Capacitor C_1 voltage variation ratio, $\sigma_1 = \frac{\Delta v_{C1}/2}{V_{C1}} > 1$

Capacitor C_2 voltage variation ratio, $\sigma_2 = \frac{\Delta v_{C2}/2}{V_{C2}} > 1$

Voltage gain, $G_{DCM} = \frac{V_2}{V_1} = \frac{D*(2-D)}{m*(1-D)^2}$

Fill factor, $m = \frac{1}{\varepsilon_1}$

Where,
V_1,V_2= input and output voltages respectively
I_1 , I_2= input and output currents respectively
D= duty ratio
T= Time period of gate pulse

Fill factor(m) is used as multiplication factor with switch turn OFF time to describe the discontinuous conduction mode of operation. Fill factor range is greater than zero and less than unity (0<m<1).

III.2.2 Comparative Analysis of various DC-DC Converter Voltage Gains

It is clear from Table 2 that traditional DC–DC converters provide a voltage gain of only up to 10. Unlike conventional converters, the ultra-lift Luo-converter offers a voltage gain greater than 10. For a wide range of output voltage operation, the ultra-lift Luo-converter is preferred because it can operate in both buck and boost modes.

Table 2: Voltage gain comparison of various DC-DC converters.

Converter	**Voltage gain formula**	**Duty Ratio**								
		0.1	**0.2**	**0.3**	**0.4**	**0.5**	**0.6**	**0.7**	**0.8**	**0.9**
Boost converter	1/(1-D)	1.11	1.25	1.43	1.67	2.00	2.50	3.33	5.00	10.00
Buck converter	D	0.10	0.20	0.30	0.40	0.50	0.60	0.70	0.80	0.90
Buck-boost converter	D/(1-D)	0.11	0.25	0.43	0.67	1.00	1.50	2.33	4.00	9.00
SEPIC converter	D/(1-D)	0.11	0.25	0.43	0.67	1.00	1.50	2.33	4.00	9.00
Ultra-lift Luo- converter	$\frac{D(2-D)}{(1-D)^2}$	0.23	0.56	1.04	1.78	3.00	5.25	10.11	24.00	99.00

Source: Authors, (2026).

The ultra-lift Luo-converter is suitable for stepping up low voltages to the desired high-voltage levels in applications such as solar energy conversion, hybrid electric vehicle chargers, and other electrical energy storage systems. The converter provides a voltage gain ranging from 0.23 (at 0.1 duty ratio) to 99 (at 0.9 duty ratio), although the 0.9 duty ratio is limited by the control switch turn-OFF period.

III.2.3 Design of Ultra-Lift Luo-Converter

The design of the ultra-lift Luo-converter involves evaluating the inductor and capacitor ratings to achieve the desired power output and output voltage for a given input voltage, without violating the allowable ripple factors of the inductor and capacitor.

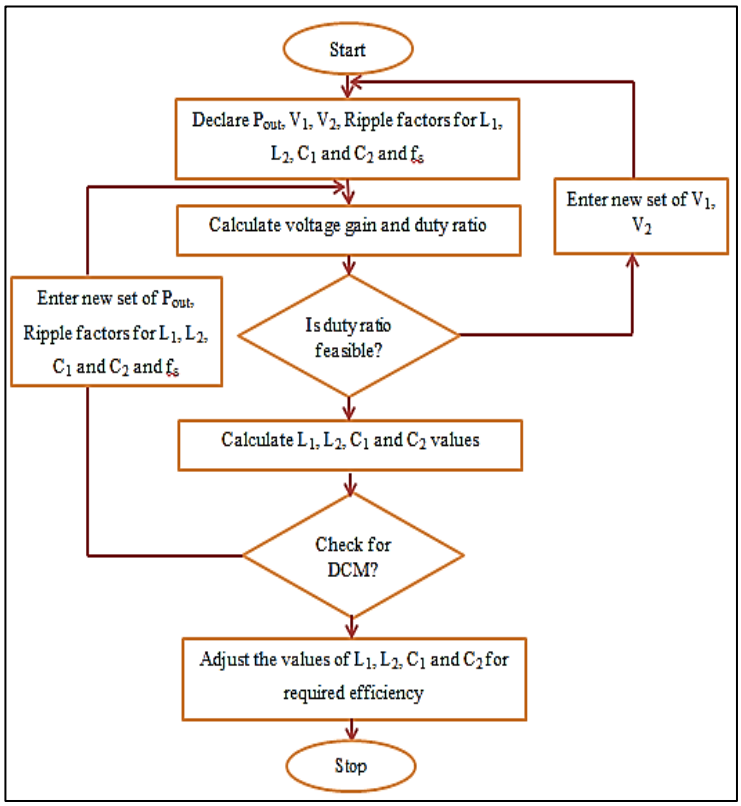

Figure 9: Flowchart for designing ultra-lift Luo-converter.
Source: Authors, (2026).

Where P_{out} = desired output power
V_1 = input voltage
V_2 = desired output voltage
L_1 and L_2 = inductor elements
C_1 and C_2= capacitor elements
f_s = switching frequency
DCM denotes Discontinuous Conduction Mode

III.2.4 Specifications of Designed Ultra-Lift Luo-Converter

Using the flowchart shown in Figure 9, the inductor and capacitor ratings are obtained by developing a MATLAB program. The designed converter specifications correspond to a power rating of 3000 W and an output voltage of 400 V DC, supplied by an input voltage of 36 V DC, with a ripple factor constraint of 0.02 for both inductors (L_1, L_2) and capacitors (C_1, C_2). The inductor and capacitor values are adjusted considering a peak conversion efficiency of 95% [11] and are further approximated to the available component ratings listed in Table 3.

Table 3: Specifications of designed ultra-lift Luo-converter.

Design Variable	Calculated Value	Chosen Value
Rated Output Power	3000 W	3000 W
Source Voltage (V_{in})	36 V	36 V
Regulated Output Voltage (V_{out})	400 V	400 V
Operating Switching Rate	50 kHz	50 kHz
Primary inductor Coil (L_1)	0.526 mH	0.5 mH
Secondary inductor Coil (L_2)	1.367 mH	1.35 mH
Input Side Filter Capacitor (C_1)	278 µF	300 µF
Output Ripple Control Capacitor (C_2)	66 µF	70 µF

Source: Authors, (2026).

III.3 BIDIRECTIONAL BUCK-BOOST CONVERTER

The bidirectional buck-boost converter can operate in both buck and boost modes, depending on the firing pulses applied to the two MOSFET switches. The converter consists of two active switches, S_1 and S_2, as shown in Figure 10. Switch S_1 is provided with pulses during the boost (discharging) mode of operation.

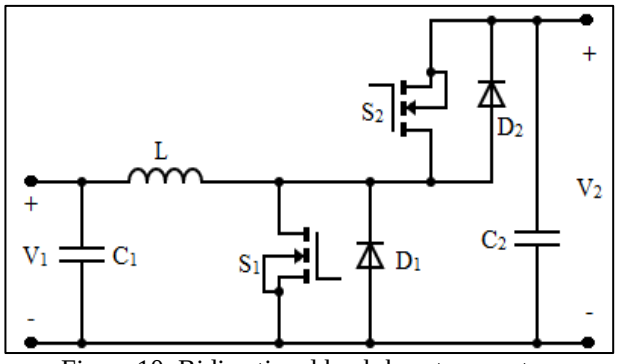

Figure 10: Bidirectional buck-boost converter.
Source: Authors, (2026).

Similarly, **S_2** is provided with pulses for bucking or charging purposes. The converter shown in Figure 10 consists of an inductor (L), capacitors (C_1 and C_2), and diodes (D_1 and D_2). V_2 is considered the voltage on the High-Voltage (HV) side, and V_1 is considered the voltage on the Low-Voltage (LV) side. Operation can be explained in two modes. They are:
1. Boost mode
2. Buck mode

1. Boost mode

In the boost mode, switch S_2 is turned OFF, and diode D_1 remains reverse-biased throughout the operation. When S_1 is turned ON, the inductor L charges, and D_2 becomes reverse-biased. Similarly, when S_1 is turned OFF, the inductor L discharges, as shown in Figure 11.

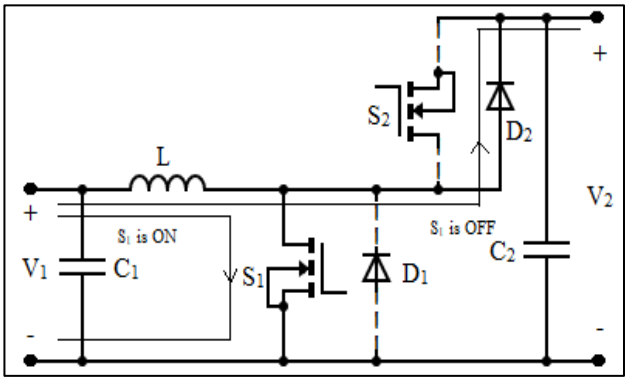

Figure 11: Bidirectional buck-boost converter in boost mode.
Source: Authors, (2026).

2. Buck mode

In the buck mode, switch **S_1** is turned OFF, and diode D_2 remains reverse-biased throughout the operation. When **S_2** is turned ON, the inductor L charges, and D_1 becomes reverse-biased. Similarly, when **S_2** is turned OFF, the inductor L discharges, as shown in Figure 12.

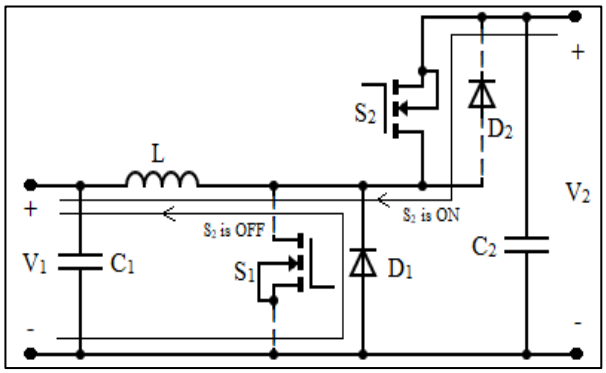

Figure 12: Bidirectional buck-boost converter in buck mode.
Source: Authors, (2026).

Analysis of Bidirectional buck-boost converter:

Duty ratio, $D_{Boost} = 1 - \frac{V_1}{V_2}$

Duty ratio, $D_{Buck} = \frac{V_1}{V_2}$

Inductor current, $I_1 = \frac{P}{V_1}$

Inductor, $L_{Boost} = \frac{D_{Boost} * V_1}{r_1 * I_1 * f_{sw}}$

Inductor, $L_{Buck} = \frac{D_{Buck} * V_2}{r_1 * I_1 * f_{sw}}$

Inductor, $L = \max(L_{Boost}, L_{Buck})$

Capacitor, $C_1 = \frac{I_2 * D_{Boost}}{r_2 * V_2 * f_{sw}}$

Capacitor, $C_2 = \frac{I_1 * D_{Buck}}{r_1 * V_1 * f_{sw}}$

Where P = Power rating

V_1 = voltage at LV side

V_2 = voltage at HV side

r_1, r_2= ripple factors

f_{sw} = switching frequency

Table 4: Specifications of Bidirectional buck-boost converter.

Parameter	Actual value	Practical Value
Output Capacity	500 W	500 W
Input Supply Level	24 V	24 V
Output DC Potential	100 V	100 V
Switching Pulse Rate	50 kHz	50 kHz
Inductor (L_1)	2.31 mH	2.5 mH
Input Filter Capacitor (C_1)	76 µF	100 µF
Output Smoothing Capacitor (C_2)	41.6 µF	50 µF

Source: Authors, (2026).

III.4 BATTERY SPECIFICATIONS

The Lithium-ion battery represented in this model has a nominal voltage of 24 V and a rated capacity of 50 Ah, suitable for medium-power applications in renewable energy storage and motor drive support. At the beginning of the simulation, the state of charge (SOC) is arbitrarily set to 45%, providing room for charging from the solar PV array and discharging to the load.

Table 5: Battery specifications.

Parameter Description	Specification
Nominal Output Voltage	24 V
Rated Energy Capacity	50 Ah
Initial Charge Level	45%
Dynamic Response Duration	1 s
Maximum Storage Capacity	50 Ah
Lower Cut-off Voltage Limit	18 V
Voltage at Full Charge	27.93 V
Typical Discharge Current	21.7391 A
Equivalent Internal Resistance	0.0048 Ω
Effective Capacity at Nominal Voltage	45.2174 Ah

Source: Authors, (2026).

III.5 BATTERY CONTROLLER

The battery controller manages the charging and discharging operations of the battery to maintain stable system performance and extend battery life. From Figure 13, the reference voltage (V_R) is compared with the actual battery voltage (V_B) to generate a voltage error as the output. This error is then fed to the voltage controller (PID controller), which determines whether charging or discharging is required.

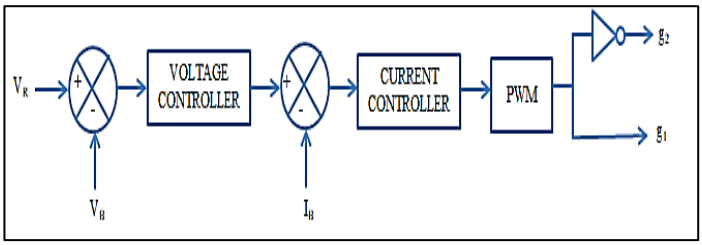

Figure 13: Battery controller block diagram.
Source: Authors, (2026).

Table 6: Battery controller specifications.

	Proportional constant (K_P)	**Integral constant (K_I)**	**Derivative constant (K_D)**
Voltage controller	0.85	10	0.005
Current controller	0.01	10	0.005

Source: Authors, (2026).

III.6 BRUSHLESS DC MOTOR

This proposed system employs a BLDC motor as the load. The BLDC motor is powered through a three-phase voltage source inverter (VSI). The inverter, in turn, responds to the regulated voltage supplied by the Ultra-Lift Luo-converter and the battery system to provide the motor with a three-phase AC supply. The electronic commutation of the BLDC motor is achieved using Hall-effect position sensors, which generate rotor position signals. Based on these signals, the inverter's switching sequence is generated, ensuring proper commutation and continuous torque production.

Table 7: Parameters of BLDC Motor.

Parameter Description	**Specification**
Stator Winding Resistance	0.7 Ω
Armature Inductance	2.72×10^{-3} H
Magnetic Flux Linkage	0.1194 Wb
Voltage (Speed) Constant	87.0946 V/krpm
Torque Generation Constant	0.84 N·m/A
Rotor Inertia	0.0002 kg·m²
Viscous Damping Coefficient	0.0004974 N·m·s
Number of Pole Pairs	4
Number of Phases	3
Back Electromotive Force (EMF) Shape	Trapezoidal
Mechanical Input Type	Torque
Back-EMF Flat Region	120°

Source: Authors, (2026).

It is a closed loop speed control system wherein the motor speed is sensed and compared with the reference speed. The motor speed thus obtained is fed to the control loop as the feedback. The error signal is processed by the PID controller to control the duty ratio of the ultra-lift Luo-converter with the Pulse Width Modulation (PWM) signal assuring the motor can run at the desired speed based upon its load and supply conditions. PID controller parameters implemented for speed control of BLDC motor are:

- Proportional constant K_P=0.2
- Integral constant K_I=8.58
- Derivative constant K_D=0.005

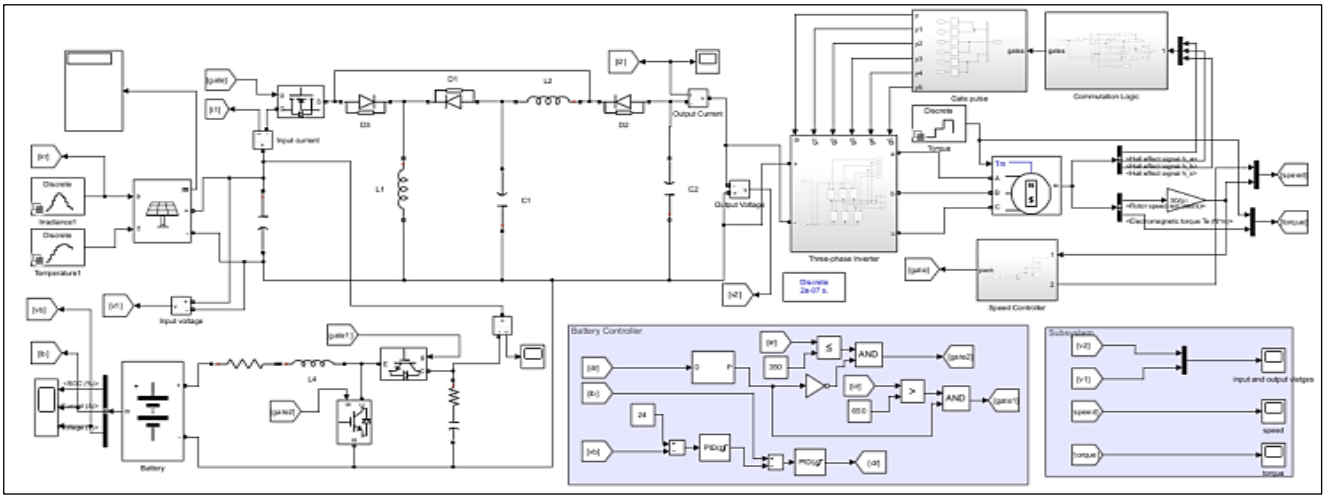

Figure 14: Proposed model of solar PV-Battery hybrid system powered BLDC motor speed control using ultra-lift Luo-converter.
Source: Authors, (2026).

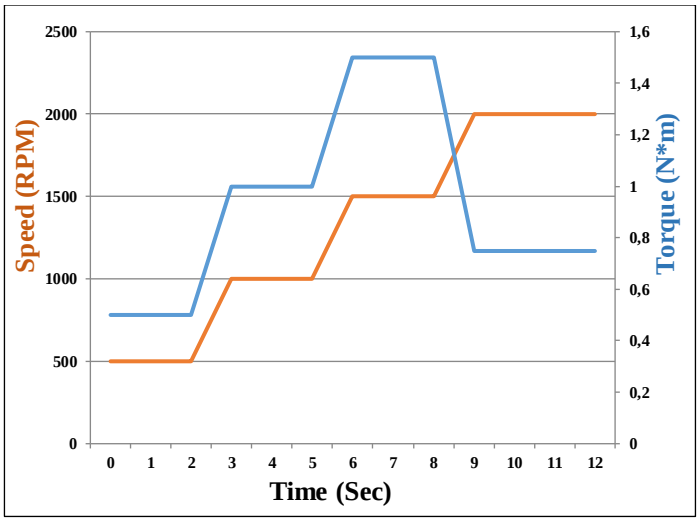

Figure 15: Speed and torque inputs to BLDC motor.
Source: Authors, (2026).

Time varying speed and torque data (Figure 15) provided as input to BLDC motor in the proposed SIMULINK model to analyse its performance of the BLDC motor.

IV. RESULTS AND DISCUSSIONS

The dynamic speed response of the BLDC motor closely follows the speed reference commands during its operation as shown in Figure 16 .

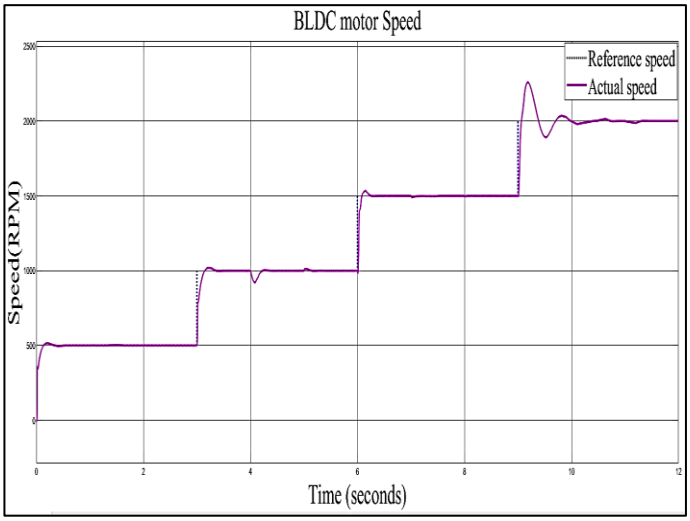

Figure 16: BLDC motor Speed.
Source: Authors, (2026).

A few transient deviations are observed during transition from one speed level to another, but the response settles down quickly to the speed reference value, indicating fast execution in the dynamics and very good steady-state performance. Even when the speed exceeds 2000 RPM, the controller tracks the reference command robustly without much oscillation. This implies good integration between the Ultra-Lift Luo-converter and the BLDC drive so as to get enough gain and solid performance from the motor.

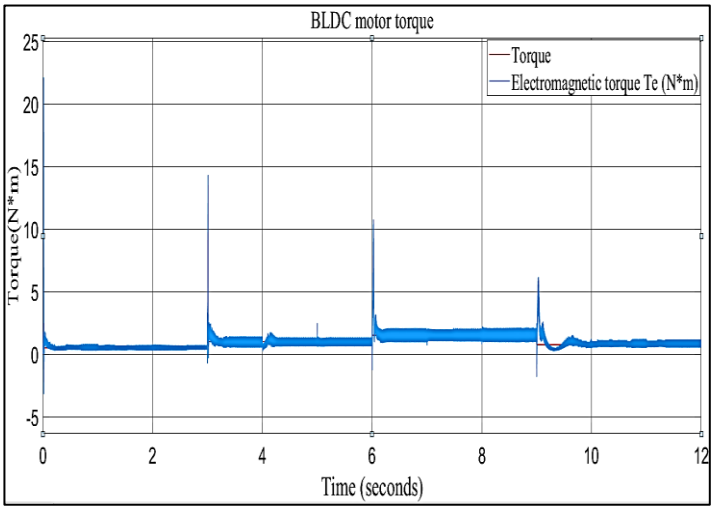

Figure 17: BLDC motor output electro mechanical torque.
Source: Authors, (2026).

The electromagnetic torque follows closely to the profile of the applied torque (Figure 17), signifying synchronization between the inverter switching sequence and motor dynamics. Due to transient oscillations, the torque gets disturbed but soon it settles back to steady values, demonstrating the capability of the controller in suppressing oscillations and ensuring steady operations of the motor. The converter output voltage increases from about 36 V to 150 V and then to almost 200 V (Figure 18) as demonstrated by the converter's ability to provide a regulated high-gain conversion when the duty ratio is varied. The output voltage settles smoothly after each transient, thereby signifying the controller's efficacy in attenuating oscillations and controlling voltage stability.

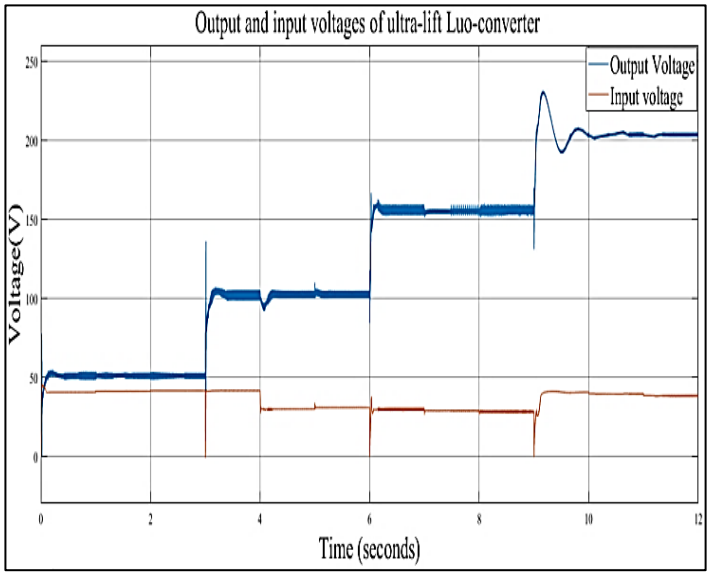

Figure 18: Output and input voltages of ultra-lift Luo-converter.
Source: Authors, (2026).

Initially the State Of Charge (SOC) profile (Figure 18) remains almost constant, indicating a balanced charging-and-discharging condition. As the converter and motor load settled down, the SOC started rising gradually, thus showing charging (4-9s) potential of the system. This gradual increase would then show that energy is efficiently transferred from the source to the battery to maintain support to load requirements.

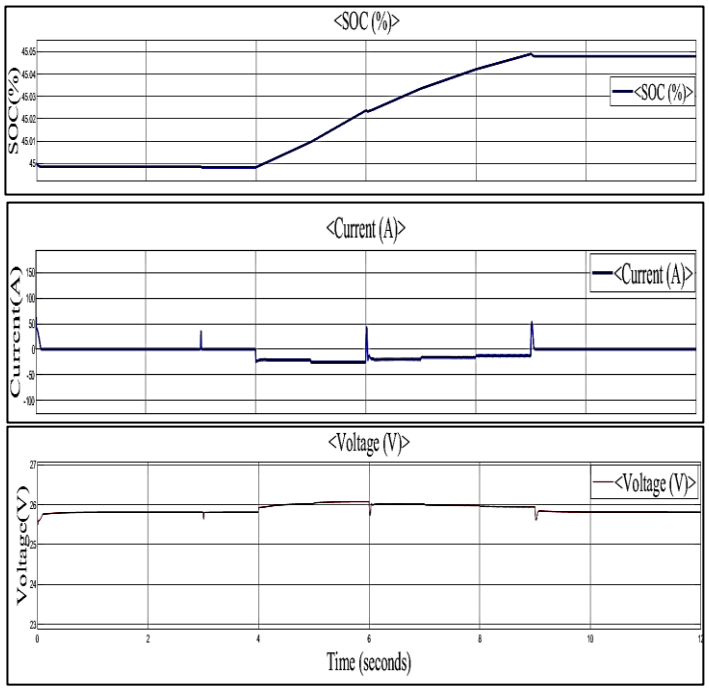

Figure 19: Battery parameter profiles: SOC, current, and voltage.
Source: Authors, (2026).

The battery voltage and current profiles (Figure 19) exhibit both positive and negative responses throughout the simulation period, demonstrating the charging and discharging behavior of the battery. Short transient spikes appear at different instances, corresponding to load and control transitions. Except for these brief occurrences, the current and voltage remain nearly constant, indicating that the controller effectively regulates both the battery current and voltage.

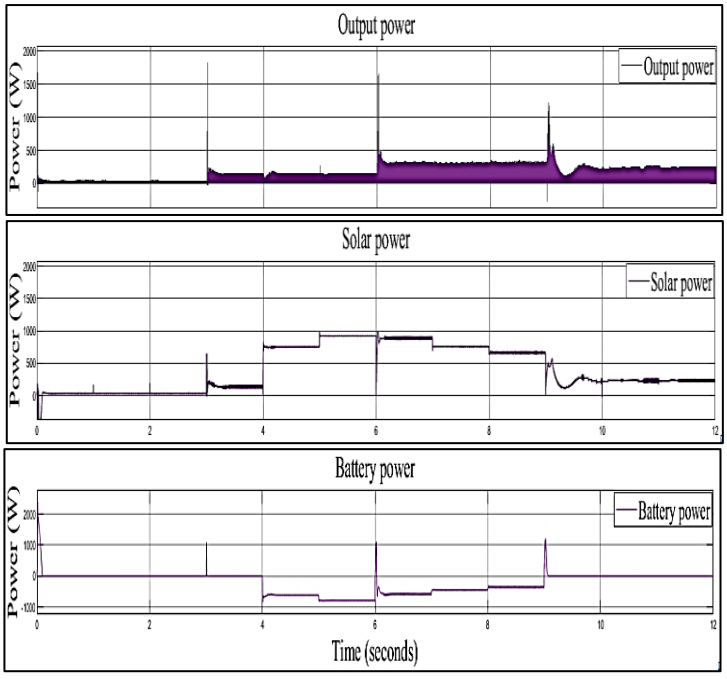

Figure 20: Power output: Ultra-lift Luo-converter, Solar PV array, and Battery.
Source: Authors, (2026).

Step changes in solar PV array output power (Figure 20) reflect variable irradiance or load conditions present upon the solar array. The solar power curve sharply rises and starts stabilizing. Between 4-6s, the array generated steadily in the range of 600–900 W, which showed reliable generation under stable irradiance. After 9 seconds, the solar output power was at a gradual decrease due decrease in irradiance and eventually stayed below 200 W, effectively making this photovoltaic source least contributory. The battery exhibits both positive and negative power values (Figure 20), confirming its bidirectional operation. After the initial transient, it delivers power to support load demand. In the periods between 4-6s, and 6-8s, the battery in fact operates in the negative region of around –500 W to –800 W, thus accounting for the charging from the excess solar generation. After 9s PV system is least effective, hence load is shared by battery.

The Ultra-Lift Luo-converter achieves the power requirements of the BLDC drive (Figure 20), even though a peak overshoot occurs initially before settling at stable power levels. The converter is able to supply a steady power output during battery switchovers and solar power inconsistencies.

V. CONCLUSIONS

The proposed ultra-lift Luo-converter is able to step up the input voltage of 36 V to voltages upto 220 V at 2000 rpm to drive the BLDC motor which is 6 times the input voltage. The motor speed response followed the reference input closely, while torque transients were suppressed by the controller. The proposed system can provide a stable DC output voltage, ensuring energy transfer to the BLDC motor under dynamic irradiance and temperature conditions. The proposed system is viable alternative for renewable energy application to ensure sustainable and reliable generation and use of clean power.

VI. AUTHOR'S CONTRIBUTION

Conceptualization: G. Dilli Harsha and Dr. Vyza Usha Reddy.
Methodology: G. Dilli Harsha and Dr. Vyza Usha Reddy.
Investigation: G. Dilli Harsha and Dr. Vyza Usha Reddy.
Discussion of results: G. Dilli Harsha and Dr. Vyza Usha Reddy
Writing – Original Draft: G. Dilli Harsha and Dr. Vyza Usha Reddy.
Writing – Review and Editing: G. Dilli Harsha and Dr. Vyza Usha Reddy.
Supervision: Dr. Vyza Usha Reddy.
Approval of the final text: G. Dilli Harsha and Dr. Vyza Usha Reddy.

VII. REFERENCES

[1] R. Kumar and M. V. Naik, "Solar PV Array Fed Zeta Converter-VSI Controlled BLDC Motor Drive for Water Pumping System," in Proceedings of the 2024 IEEE Students Conference on Engineering and Systems (SCES), 2024. DOI: 10.1109/SCES61914.2024.10652421

[2] R. Kumar and B. Singh, "Solar PV-battery based hybrid water pumping system using BLDC motor drive," in Proc. 2016 IEEE 1st Int. Conf. on Power Electronics, Intelligent Control and Energy Systems (ICPEICES), Delhi, India, 4-6 July 2016, pp. 1-6, doi: 10.1109/ICPEICES.2016.7853662. DOI: 10.1109/ICPEICES.2016.7853662

[3] U. K. Kalla, S. P. S. Rajawat, S. Singh and N. Bhati, "Solar PV-fed Battery-Powered PMBLDCM driven Water Pumping System using Cuk Converter," in Proceedings of the 2021 IEEE 2nd International Conference on Smart Technologies for Power, Energy and Control (STPEC), Bilaspur, Chhattisgarh, India, 2021, pp. 1–6. DOI: 10.1109/STPEC52385.2021.9718691.

[4] N. H. Nimer, H. Al-Mattarneh, J. Kumar IJ, et al., "Coordinated Power Management for Speed Control of BLDC Motor Powered by Wind–Battery–PV for Water Pumping Applications", Proceedings of the 2024 IEEE International Conference on Sustainable Power & Energy (ICSPE), 2024. DOI: 10.1109/ICSPE62629.2024.10924359.

[5] Rajan Kumar, Bhim Singh, Ambrish Chandra, Kamal Al-Haddad, "Solar PV Array Fed Water Pumping Using BLDC Motor Drive with Boost-Buck Converter", IEEE Energy Conversion Congress and Exposition (ECCE), pp 5741-5748, 2015. DOI: 10.1109/ECCE.2015.7310466

[6] F.L. Luo and H. Ye, "Ultra-lift Luo-converter", 2004 International Conference on Power System Technology, Vol. 152, No. 1, pp. 27-32, January 2005.F. L. Luo and H. Ye, DOI: 10.1109/ICPST.2004.1459970

[7] F. L. Luo and H. Ye, "Positive Output Super-lift Converters", IEEE Transactions on Power Electronics, vol. 18, no. 1, pp. 105-113, Jan. 2003. DOI: 10.1109/TPEL.2002.807198

[8] A. Vishnu Kumar, Dr. V. Jayalakshmi, "Modelling of Ultra-Lift Luo Converter Using PI Controller for Stand Alone Application", International Conference on Intelligent and Innovative Technologies in Computing, Electrical and Electronics (IITCEE), pp 1-4, 2024. DOI: 10.1109/IITCEE59897.2024.10467422

[9] A. Sharifian, S. F. Sasansara, M. J. Ghadi, S. Ghavidel and L. Li, "Dynamic performance improvement of an ultra-lift Luo DC–DC converter by using a type-2 fuzzy neural controller," Computers & Electrical Engineering, vol. 69, pp. 171-182, 2018, DOI:https://doi.org/10.1016/j.compeleceng.2018.05.012

[10] Pearl Nightingale.R.H, Dr. Mrunal Deshpande, "Design of Ultra lift Luo Converter using Incremental Conductance Technique for PV Application", 2nd International Conference on Power and Embedded Drive Control (ICPEDC), pp 201-207, 2019. DOI: 10.1109/ICPEDC47771.2019.9036619

[11] Jeff Falin, Designing DC/DC converters based on ZETA topology, Texas Instruments Incorporated, 2010.